

Air-stable and oriented mixed lead halide perovskite (FA/MA) by one-step deposition method using zinc iodide and chloroamine additive

Loreta A. Muscarella, Dina Petrova, Rebecca Jorge Cervasio, Aram Farawar, Olivier Lugier, Charlotte McLure, Martin J. Slaman, Junke Wang, Bruno Ehrler, Elizabeth von Hauff, and Rene M. Williams

ACS Appl. Mater. Interfaces, **Just Accepted Manuscript** • DOI: 10.1021/acsami.9b03810 • Publication Date (Web): 16 Apr 2019Downloaded from <http://pubs.acs.org> on April 17, 2019**Just Accepted**

“Just Accepted” manuscripts have been peer-reviewed and accepted for publication. They are posted online prior to technical editing, formatting for publication and author proofing. The American Chemical Society provides “Just Accepted” as a service to the research community to expedite the dissemination of scientific material as soon as possible after acceptance. “Just Accepted” manuscripts appear in full in PDF format accompanied by an HTML abstract. “Just Accepted” manuscripts have been fully peer reviewed, but should not be considered the official version of record. They are citable by the Digital Object Identifier (DOI®). “Just Accepted” is an optional service offered to authors. Therefore, the “Just Accepted” Web site may not include all articles that will be published in the journal. After a manuscript is technically edited and formatted, it will be removed from the “Just Accepted” Web site and published as an ASAP article. Note that technical editing may introduce minor changes to the manuscript text and/or graphics which could affect content, and all legal disclaimers and ethical guidelines that apply to the journal pertain. ACS cannot be held responsible for errors or consequences arising from the use of information contained in these “Just Accepted” manuscripts.

1
2
3 **Air-stable and oriented mixed lead halide perovskite (FA/MA) by one-step**
4 **deposition method using zinc iodide and chloroamine additive**
5
6
7
8
9

10 Loreta A. Muscarella,^{1,4} Dina Petrova,¹ Rebecca Jorge Cervasio,¹ Aram Farawar,¹
11 Olivier Lugier,¹ Charlotte McLure,¹ Martin J. Slaman,² Junke Wang,³ Bruno Ehrler,⁴
12 Elizabeth von Hauff,² René M. Williams*¹
13
14
15
16
17
18

19 ¹ Molecular Photonics Group, Van't Hoff Institute for Molecular Sciences (HIMS),
20 Universiteit van Amsterdam, Science Park 904, 1098 XH Amsterdam, Netherlands
21
22

23 ² Department of Physics and Astronomy, Vrije Universiteit, de Boelelaan 1081, 1081
24 HV Amsterdam, Netherlands
25
26
27

28 ³ Molecular Materials and Nanosystems, Eindhoven University of Technology, P.O.
29 Box 513, 5600 MB Eindhoven, Netherlands
30
31
32

33 ⁴ Center for Nanophotonics, Institute AMOLF, Science Park 104, 1098 XG Amsterdam,
34 Netherlands.
35
36
37
38
39
40
41
42
43
44
45
46
47
48
49
50
51
52

53 AUTHOR INFORMATION

54 **Corresponding Author**

55
56
57
58 * R.M.Williams@uva.nl
59
60

Abstract:

We present a one-step method to produce air-stable, large grain mixed cationic lead perovskite films and powders under ambient condition. The introduction of 2.5 wt% of Zn(II), confirmed by X-Ray Diffraction (XRD), results in stable thin films which show the same absorption and crystal structure after two weeks of storage under ambient conditions. Next to prolonged stability, the introduction of Zn(II) affects photo-physical properties reducing the bulk defect density, enhancing the photoluminescence and extending the charge carrier lifetime. Furthermore, 3-chloropropylamine hydrochloride (3-CPACl) is applied as film-forming agent. The presence of this amine hydrochloride additive results in highly oriented and large crystal domains showing an ulterior improvement of photoluminescence intensity and lifetime. The material can also be prepared as a black precursor powder by a solid-solid reaction under ambient conditions and can be pressed into a perovskite pellet. The prolonged stability and the easy fabrication in air makes this material suitable for large scale, low cost processing for optoelectronic applications.

Keywords: photovoltaics, hybrid perovskite, formamidinium, methylammonium, 3-chloropropylamine chloride, zinc iodide, chloride additive

Introduction

The rise of the power conversion efficiency of perovskite solar cells (PSC) from 3.8%¹ to 24.2% in 10 years has shaken up the scientific photovoltaic community. Breakthroughs in the efficiency have largely come from new strategies to fabricate perovskite thin films. Currently, improving the stability of perovskite films is a major challenge in the field.² Comprehensive understanding and control of the inherent photochemical properties affecting stability of these intriguing materials is therefore paramount for further progress.³

The chemical landscape of perovskites for solar cells is limited to basically eight main components: methylammonium (MA), formamidinium (FA), cesium (Cs) as monovalent cations, Pb(II) and Sn(II) as divalent species and chloride, bromide and iodide as anions. The intrinsic properties of MAPbI₃ and FAPbI₃ prohibit their use as pure materials for industrial applications such as solar cells, as they do not have suitable chemical stability due to their phase-behavior.⁴ MAPbI₃ displays a cubic to tetragonal phase transition at approximately 57°C, and slowly turns white (MAPbI₃·H₂O) or yellow (MA₄PbI₆·2H₂O) when exposed to a humid atmosphere. The FAPbI₃ cubic black α -phase interconverts to the non-perovskite, hexagonal yellow δ -phase in a couple of weeks in dry air at RT.⁵

Significant improvements have been observed by mixing anions or cations. Incorporation of a small amount of bromide (or chloride) influences the phase-changes while the band gap remains unchanged, as already reported for MAPbI_{2.66}Br_{0.34} by Weber in 1978⁶. However, chloride components in the precursor solutions tend to be mainly eliminated as HCl vapor (or as CH₃NH₃Cl) during the annealing step through an intermediate phase, if an excess iodide is present (less than 1% chloride in final phase).⁷

1
2
3 The most recent power conversion efficiency (PCE) records were obtained with
4 (FA/MA) double (22.1% and 20.2%),⁸ (FA/MA/Cs) triple (21.1%)⁹ and
5
6 (FA/MA/Cs/Rb) quadruple (21.6%)¹⁰ mixed mono-cationic lead iodide materials.
7
8

9
10 So far, Sn(II) is the only divalent metal cation that can result in semiconductors
11 of similar bandgap and electron and hole transport properties as the Pb(II) equivalent,
12 but it suffers from rapid degradation due to its chemical instability in air.
13
14

15
16 Doping of traditional semiconductors is quintessential for their application in
17 optoelectronics devices, therefore it is tempting to dope Pb(II) perovskite thin films
18 with various other ions. Monovalent cation like Cu(I), Na(I), and Ag(I)¹¹ as well as
19 Au(III), In(III) and Al(III)¹² and Sr(II)¹³ have been applied as dopants, and more
20 recently Zn(II).^{14,15,16} It has been found that for these materials, small doping levels
21 with respect to Pb give maximum enhancement of optoelectronic properties with
22 minimal structural modification. Furthermore, the use of additives that influence film
23 formation¹⁷ are of great importance. Additives with alkyl-ammonium groups have been
24 shown to influence stability of perovskite materials¹⁸ by interacting with the perovskite
25 crystal surface.
26
27
28
29
30
31
32
33
34
35
36
37
38
39
40
41

42 Here, we study the effect of Zn(II) on the photophysical properties of the mixed
43 cations and mixed halides (FA_{0.85}MA_{0.15})Pb(I_{0.85}Br_{0.15})₃ perovskite thin films made by
44 one-step deposition in air. In addition, we apply an amine hydrochloride additive to our
45 perovskite and its effect on film formation and morphology is studied. The introduction
46 of Zn(II) results in a prolonged film stability under ambient condition, enhanced
47 photoluminescence and extended lifetime, without affecting the band gap. The main
48 challenge for producing perovskite films from a solution is to obtain a uniform,
49 continuous, and compact layer. For this purpose, a common and straightforward method
50
51
52
53
54
55
56
57
58
59
60

1
2
3 is to apply chloride-based additives. In this study, we apply 3-chloropropylamine
4 hydrochloride (3-CPACl) which allows to produce highly crystalline oriented, smooth,
5 dense and pinhole-free layers. Furthermore, the perovskite can also be prepared from
6 our precursor as a pellet-able black powder by a solid-solid reaction under ambient
7 conditions.
8
9
10
11
12
13
14
15
16

17 **Experimental**

18
19 **Materials.** 3x3 cm² patterned Indium Tin Oxide (ITO) with a sheet resistance
20 of 13-15 Ω/sq, was purchased from Ossila. PbI₂ (99%), ZnI₂ (98%), 3-
21 chloropropylamine hydrochloride (3-CPACl, 98%) were purchased from Sigma-
22 Aldrich. Methylamine hydrobromide (MABr, 98%), Formamidinium hydroiodide (FAI,
23 98%) were purchased from TCI. N,N-dimethylformamide (DMF) was purchased from
24 Biosolvie Chimie SARL.
25
26
27
28
29
30
31
32

33 **Preparation of the (FA_{0.85}MA_{0.15})Pb(I_{0.85}Br_{0.15})₃-based solutions.** MABr
34 (1.2M), FAI (1.2 M), PbI₂ (1 M) were dissolved in DMF with a mole ratio of 1:1:1. In
35 order to study the effect of Zn(II), 2.5 wt% of ZnI₂ was also added. A third precursor
36 solution was prepared including 2.5 wt% of ZnI₂ and 2% of 3-CPACl to study the effect
37 of the amine hydrochloride additive in combination with the Zn(II).
38
39
40
41
42
43

44 **Fabrication and Characterization of the thin films.**

45 (FA_{0.85}MA_{0.15})Pb(I_{0.85}Br_{0.15})₃ films were fabricated on ITO and quartz substrates and
46 the pure (FA_{0.85}MA_{0.15})Pb(I_{0.85}Br_{0.15})₃ was used as a comparison. ITO and glass were
47 cleaned by ultrasonication in water, acetone and 2-propanol sequentially, dried with air
48 flow and UV-ozone treated for 30 minutes. Before spin coating, a N₂ flow is blown
49 over the surface to remove dust or particles. Without the 3-CPACl additive, the
50 precursor solution results in a yellow milky solution due to the low solubility of PbI₂ in
51
52
53
54
55
56
57
58
59
60

1
2
3 DMF. To remove PbI_2 particles, the solution has to be filtered using a 0.2 μm syringe
4 filter. Filtration is not necessary in presence of the additive. Each of the solutions was
5
6 spin-coated on the substrates with a speed of 4000 rpm for 30 s under ambient condition
7
8 (no acceleration factor was applied). The one-step deposition method with sprayed anti-
9
10 solvent (diethylether, DEE) was used. After 15 seconds from start of the spin-coating
11
12 programme, 0.4 mL of DEE was sprayed within ~ 0.5 s over the precursor perovskite
13
14 layer at a fixed height of 3 centimetres between the needle tip and the surface. A metal
15
16 gasket from an HPLC setup was used as a height fixation. After the spin-coating, thin
17
18 films were annealed at 100 $^\circ\text{C}$ for 1 hour.
19
20
21
22
23

24 The stability in time of the perovskite layers was measured by monitoring Uv-
25
26 Vis spectra and X-Ray diffraction (XRD) after two weeks under ambient conditions
27
28 and without encapsulation. XRD measurements were performed to investigate the
29
30 introduction of Zn(II) in the perovskite lattice. The morphology and EDS spectra of
31
32 the films were characterized by using a scanning electron microscopy (SEM). Steady-
33
34 state photoluminescence (PL) was measured with a home-built setup equipped with a
35
36 485 nm continuous-wave laser as source of excitation (Pico Quant LDH-D-C-640) at a
37
38 power output of 1 mW. Time-correlated single photon counting (TCSPC)
39
40 measurements were performed with a home-built setup equipped with a 485 nm pulsed
41
42 laser (PicoQuant LDH-D-C-640) with a repetition rate of 0.1 MHz.
43
44
45
46
47
48
49
50
51
52
53
54
55
56
57
58
59
60

Results and discussions

The enhanced stability of the mixed cationic $(\text{FA}_{0.85}\text{MA}_{0.15})\text{Pb}(\text{I}_{0.85}\text{Br}_{0.15})_3$ perovskite compared to its single-cation and iodide-based counterparts fabricated under inert conditions was already studied before¹⁹. In the text we refer to $(\text{FA}_{0.85}\text{MA}_{0.15})\text{Pb}(\text{I}_{0.85}\text{Br}_{0.15})_3$ as pristine material. Here, we study the effect of the introduction of a small amount (2.5 wt%) of the divalent transition metal Zn(II) in the mentioned above perovskite fabricated under ambient condition. The theoretical Goldsmith tolerance factor (t) for a generic ABX_3 perovskite is calculated as shown in Eqn (1).

$$t = \frac{r_A + r_X}{\sqrt{2}(r_B + r_X)} \quad (1)$$

Here, r_A , r_B , and r_X are the ionic radii for the cation (A), metal (B), and halide (X) sites, respectively. If the tolerance factor is in the range 0.813–1.107, perovskites do form²⁰. Weighing the contribution of the two A^+ cations and X^- anions (15:85 MA^+/FA^+ and Br^-/I^- ratio) and the two B^{2+} cations (0.025:0.975 $\text{Zn}^{2+}/\text{Pb}^{2+}$ ratio), the resulting Goldsmith tolerance factor for the perovskite containing 2.5 wt% Zn(II) is 0.981 compared to 0.978 for the full Pb-perovskite, in agreement with the smaller ionic radius shown by Zn(II) (74 pm) compared to Pb(II) (119 pm).

The introduction of Zn (II) does not affect significantly the typical X-Ray Diffraction (XRD) pattern shown by the pristine material which results in a pseudocubic crystal structure (**Figure 1a**) as reported before for this material⁸. To corroborate the presence of Zn (II) in the perovskite lattice, which presumably occupies Pb^{2+} sites, the magnification of the two highest diffraction peaks are shown in **Figure 1b**. Both peaks show a 0.05° 2θ shift to higher values indicating a contraction of the elementary cell in agreement with the smaller ionic radius of Zn (II). The (110) peak shifts from 13.89° to 13.94° while the (220) peak shifts from 28.09° to 28.13° . As result,

the pseudo-cubic lattice parameter is reduced from 6.3710 Å to 6.3474 Å. With Zn(II) introduction, the material shows an improved crystallinity supported by the FWHM value reduction from 0.2799 to 0.1877.

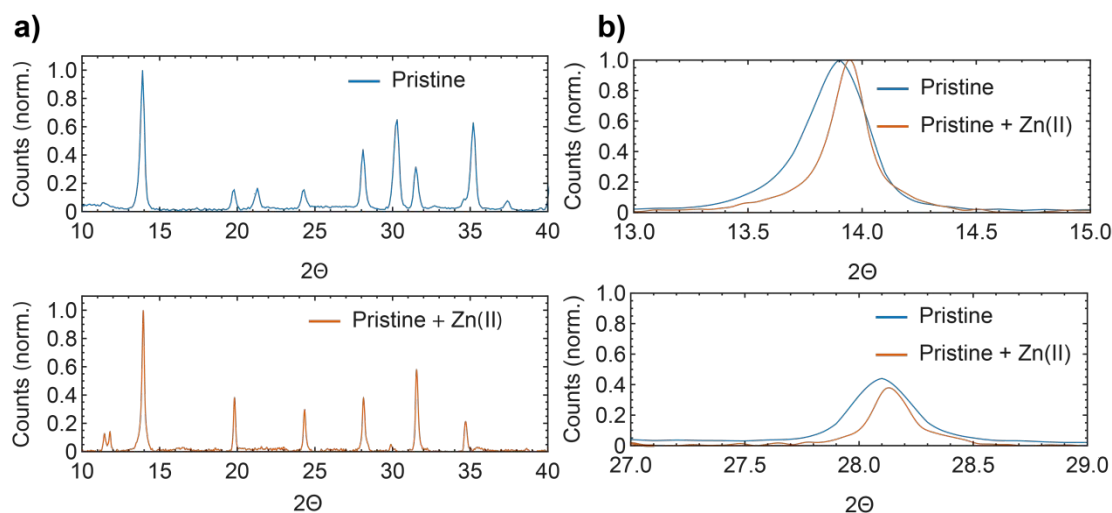


Figure 1. a) XRD patterns of the pristine perovskite compared to the pristine containing Zn(II). **b)** Magnification of the two highest diffraction peaks corresponding to the (110) and (220) planes. The shift to higher 2θ indicates the incorporation of Zn(II).

For higher weight concentration of ZnI_2 (5 wt%), UV-Vis absorption measurements indicate no change in the band gap, but XRD pattern (**Figure S1**) shows a stronger PbI_2 peak at 12.55° in addition to extra diffraction peaks which suggest less oriented crystal domains and the presence of more FAPbI_3 δ -phase (11.47° , 21.13° and 30.17°)¹⁹.

ZnI_2 is a very hygroscopic salt but it leads to higher stability against environmental moisture when introduced in our perovskite as Zn(II).

One of the causes of perovskite degradation is attributed to the oxidation of I⁻ to I₂ in aprotic solvent which introduces deficiency in I/Pb stoichiometry as reported for MAPbI_3 but also for other iodide-based perovskite^{21,22}. For this process, moisture is

1
2
3 essential, and the degradation is accelerated under various stresses, such as oxygen
4 presence, light illumination or applied bias. This degradation starts with uncontrolled
5 incorporation of moisture during the fabrication and for this reason it is advisable to
6 fabricate devices in low humidity environment. The use of a reducing agent to prevent
7 I_2 formation was shown by Zhang et al. using hypophosphorous acid (HPA) as
8 additive²³. ZnI_2 , which is present in the precursor solution as Zn^{2+} and I^- , is a stronger
9 reducing agent compared to HPA, and reacts with the I_2 formed in solution during the
10 fabrication reducing defects in the stoichiometry and leading to a more stable
11 perovskite. The reduced defect density is also reflected in the enhanced
12 photoluminescence shown later in this work.

13
14
15
16
17
18
19
20
21
22
23
24
25
26
27
28
29
30
31
32
33
34
35
36
37
38
39
40
41
42
43
44
45
46
47
48
49
50
51
52
53
54
55
56
57
58
59
60

The stability of thin films is monitored by comparing UV-Vis absorption spectra and XRD patterns of freshly-made and aged films. The aged ones were measured after 14 days of storage in a Petri dish under ambient conditions of our chemical laboratory where the ambient temperature is $(21.0 \pm 2)^\circ C$ and the relative humidity (%RH) is 40 ± 4 . The pristine material starts to degrade within the first week showing a progressive color change from black (perovskite α -phase) to a complete light-yellow color after 30 days (PbI_2). This degradation is confirmed by the enhancement of the PbI_2 absorption peak in the Uv-Vis range (~ 550 nm) and the increase of the diffraction feature related to the (001) plane of lead iodide at 12° (2θ). The XRD pattern related to the aged pristine material shows also broader peaks and the presence of new diffraction peaks due to the reduced crystallinity and less oriented crystal domains (**Figure S2a, b**). The degradation is not reversible, and the perovskite α -phase is not recovered after re-annealing. As shown in **Figure 2a**, the aged perovskite containing Zn (II) shows the same XRD pattern as the freshly-made and a slight reduction in crystallinity, visible by

the widening of the FWHM diffraction peak, which is presumably due to the interaction of the perovskite layer (not encapsulated) with the environmental humidity.

The absorption, shown in **Figure 2b**, does not show significant changes compared to the freshly-made film. Combining these results with the visual degradation of thin films over time (*inset* in **Figure 2a**), we conclude that Zn(II) incorporation stabilizes our perovskite against environmental moisture.

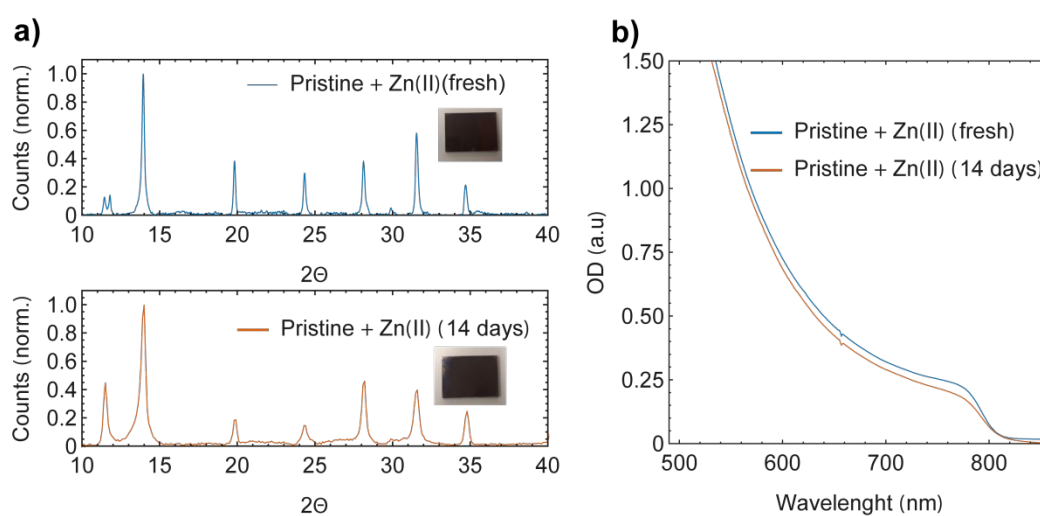


Figure 2. **a)** X-Ray diffraction (XRD) patterns of freshly-made and aged pristine perovskite containing Zn(II). Inset, photographs of fresh and aged sample are reported. **b)** UV-Vis absorption spectrum of the freshly-made and aged pristine perovskite containing Zn(II).

A major challenge in the perovskite field is to obtain uniform, continuous and reproducible films by spin-coating deposition with the use of antisolvents. A large number of pinholes are generated during the film formation and long optimisation processes dependent on substrates, precursor solutions, deposition conditions are necessary before to obtain appreciable results. In recent years, many works were focused on finding tricks to circumvent this issue and most of the time chloride-based

additives^{24,25,26} are applied. Despite the stability improvement, our thin films suffer of pinholes and inhomogeneity as shown in the SEM image in **Figure S3**. As the deposition occurs under ambient conditions without control of parameters as temperature, humidity or air-flow it was necessary finding a straightforward method to obtain reproducible and pinhole-free layers.

We found an excellent film formation with 3-chloropropylamine hydrochloride (3-CPACl), characterized by a propylic chain at whose ends an amine group and a chloride are present. Thus, we introduce 2% of 3-CPACl in the solution of the pristine perovskite containing Zn(II). The acidic part of 3-CPACl improves solubility of PbI₂ in DMF, as also observed for other additives as HI²⁷, HPA²³, formic acid²⁸, while the chloride bound to the propylic chain (acting as a soft Lewis base) chelates temporarily the Pb²⁺ atom (acting as a soft Lewis acid) in solution (**Figure 3a**), thus aiding crystals growth. We propose that a gradual change of the ratio of (FA/MA) relative to CPACl during spin-coating and annealing (**Figure 3b,c**) induces crystals orientation while the additive is removed by thermal annealing, resulting in a compact and oriented layer (**Figure 3d**). A controlled ratio-change of similar components was reported by Mitzi and co-workers with Sn(II) and n-butylammonium²⁹.

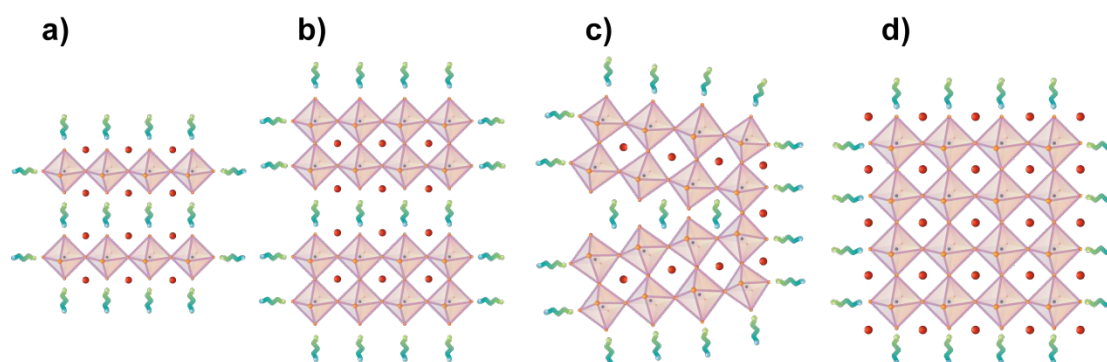


Figure 3. Proposed mechanism for additive-assisted film formation. Decreasing of additive/perovskite ratio during spin-coating and annealing (**a, b, c**) leads to stacking

1
2
3 *of preformed crystalline units coordinated by 3-CPACl through the Pb-Cl bond*
4 *resulting in an organized and compact final perovskite layer (d). The green structure*
5 *represents the additive which coordinates Pb²⁺ in the perovskite unit cell*
6
7
8
9
10
11

12 Deposition of precursor solution containing Zn(II) and 3-CPACl results in dark
13 brownish films immediately after spin-coating, as indicated in **Figure S4** which
14 displays a highly smooth and reflective film with full surface coverage. It is worthwhile
15 to mention that the pure MA/FA-Pb-I_xBr_y only turns black upon thermal annealing.
16
17
18
19
20

21 As shown in **Figure 4a**, the 3-CPACl additive induces crystal orientation and
22 highly oriented and stable pseudo-cubic structure as only the specific diffractions
23 corresponding to the (100) and (200), at 14.04° and 28.24°, remain. To estimate the
24 crystallite sizes, Scherrer equation was applied to the most intense peak (100) in the
25 XRD pattern. The average crystallite size in the pristine perovskite, in the perovskite
26 containing Zn(II) and in the one containing Zn(II) and treated with 3-CPACl was found
27 to be 36, 54 and 114 nm respectively, indicating an enlargement in size of the perovskite
28 crystallites.
29
30
31
32
33
34
35
36
37
38
39

40 To support the role of 3-CPACl in the crystal growth, the pristine material
41 containing only the film-forming agent reveals an average crystallite size of 87 nm,
42 which is almost three times of the crystallite size of the pristine material. A detailed
43 summary of the calculated FWHM and crystallite size for the different materials is
44 reported in **Table S1**. It is important to note that the Scherrer equation gives a rough
45 estimation of crystallite size and is only valid for particles smaller than 0.1 μm.
46
47
48
49
50
51
52

53 To strengthen the role of 3-CPACl as film-forming agent, **Figure 4b** shows Scanning
54 Electron Microscopy (SEM) image of a typical layer containing Zn(II) and treated with
55 3-CPACl deposited on ITO. SEM image indicates a dense, homogeneous and pinhole-
56
57
58
59
60

1
2
3 free layer. High resolution images of our films show ~500 nm perovskite grains (**Figure**
4 **S5**). We note that apparent grain boundaries in the SEM do not necessarily represent
5 crystal grain boundaries but could be purely morphological. The SEM images are thus
6 not contradicting the grain size extracted from XRD.
7
8
9
10

11
12 To verify if the prolonged stability shown by the pristine perovskite containing
13 Zn(II) is also maintained in presence of 3-CPACl, Uv-Vis absorption spectra (**Figure**
14 **S6**) and XRD (Figure 4a) patterns of freshly-made and aged films are collected. The
15 aged samples were measured after 60 days of storage in a Petri dish under ambient
16 conditions of our chemical laboratory where the ambient temperature is $(21.0\pm 2)^\circ\text{C}$
17 and the relative humidity (%RH) is 40 ± 4 .
18
19
20
21
22
23
24
25

26 Also, our Zn(II) doped spin-coated films made with the 3-CPACl additive remain in its
27 α -phase even after 60 days under ambient conditions. We correlate the prolonged
28 stability under ambient condition to the combined action of the two additives: the
29 preferential orientation and the grain enlargement induced by the film-forming agent
30 reduces the amount of dangling bonds usually present at the grain boundaries, while
31 the presence of Zn(II) can passivate Pb^{2+} vacancies and reduce the amount of I
32 vacancies by striking the conversion of I⁻ to I₂ in the precursor solution.
33
34
35
36
37
38
39
40
41

42 After 60 days the FWHM is slightly increased from $0.09315^\circ\pm 0.0004^\circ$ to
43 $0.1956^\circ\pm 0.0004^\circ$ while the ratio between the (100) and (200) diffraction peaks in the
44 freshly-made and in the aged sample is maintained. The $\Delta(\text{FWHM})$ between the fresh
45 and the aged sample is 0.1612° in the case of the pristine material containing only Zn(II)
46 and it is reduced to 0.10245° when 2% of 3-CPACl is applied.
47
48
49
50
51
52
53

54 As result of these findings we can confirm that the prolonged stability is
55 preserved and improved when ZnI_2 is used in combination with 3-CPACl.
56
57
58
59
60

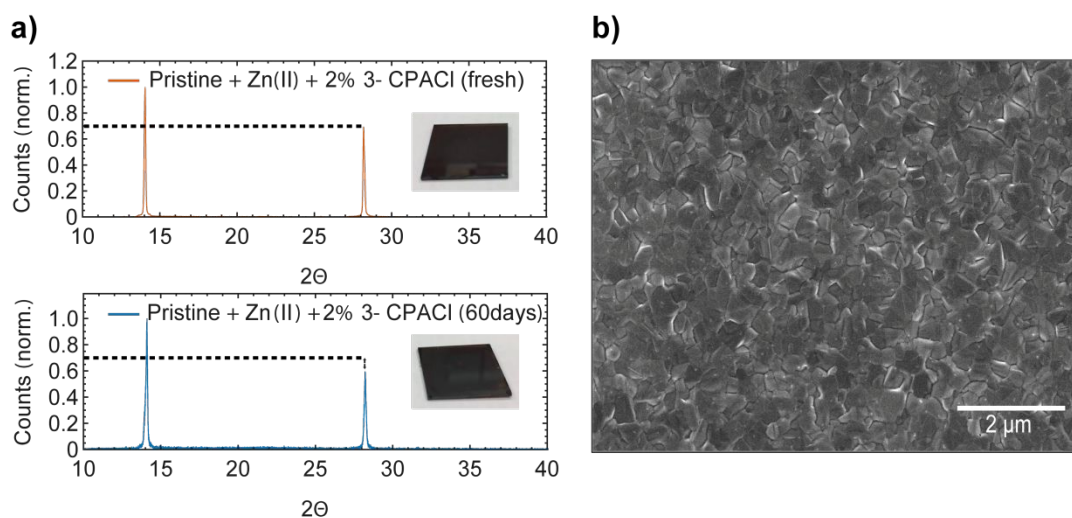


Figure 4. **a)** XRD patterns of freshly-made and aged perovskite containing Zn(II) and 3-CPACI. Inset pictures films before and after aging. **b)** Low magnification (20000x) SEM image of perovskite containing Zn(II) and 3-CPACI showing homogeneous, dense and pinhole free layer.

Although Energy Dispersive X-ray (EDX) analysis clearly shows the presence of Zn, Br, Pb and I (**Figure S7**), we find no evidence of Cl. If the chloride not bound to the propylic chain of the additive is introduced in the material, its amount is below the detection limit of the EDX. As reported also by other works, the chloride introduced to perovskite as additive or dopant, often disappears during perovskite formation as HCl or MnCl^{30} .

However, a magnification of the pristine and the material containing Zn(II) and 3-CPACI diffraction pattern (**Fig. 5a**) shows a shift towards higher 2θ values (14.04°) indicating a contraction of the primitive cell to 6.3027\AA which can be related to the incorporation of chloride in I⁻ sites. A summary of the lattice parameters reported in the text is shown in **Table S2**.

1
2
3 The use of a very similar amine hydrobromide additive (3-BPABr = 3-
4 bromopropylamine hydrobromide) results in a highly oriented film which shows the
5 same preferential orientation along the (100) and the (200) plane shown using 3-
6 CPACl. This corroborates the role of the propylic chain bound to a halide atom into the
7 crystal growth. Diffraction peaks show a shift to higher 2θ values for the perovskite
8 treated with 3-BPABr. In particular the (100) diffraction shifts from 13.89° to 14.09°
9 and the (200) diffraction shifts from 28.09° to 28.29° , and the lattice parameter
10 decreases to 6.2783\AA (**Figure 5a**). This finding is also confirmed by the strong shift of
11 the band gap to higher energy, indicating the incorporation of the bromide in the lattice
12 as shown in **Figure 5b**. The absorption edge of our perovskite containing Zn(II) and 3-
13 CPACl is around 830 nm, in agreement with FA/MA Pb-based perovskite mostly
14 containing formamidinium and iodide. The absorption in the 750-830 nm region shows
15 a significant enhancement, and we assume that the perovskite surface morphology and
16 coverage induced by the presence of the film-forming agent play an important role in
17 it.
18
19
20
21
22
23
24
25
26
27
28
29
30
31
32
33
34
35
36
37
38
39
40
41
42
43
44
45
46
47
48
49
50
51
52
53
54
55
56
57
58
59
60

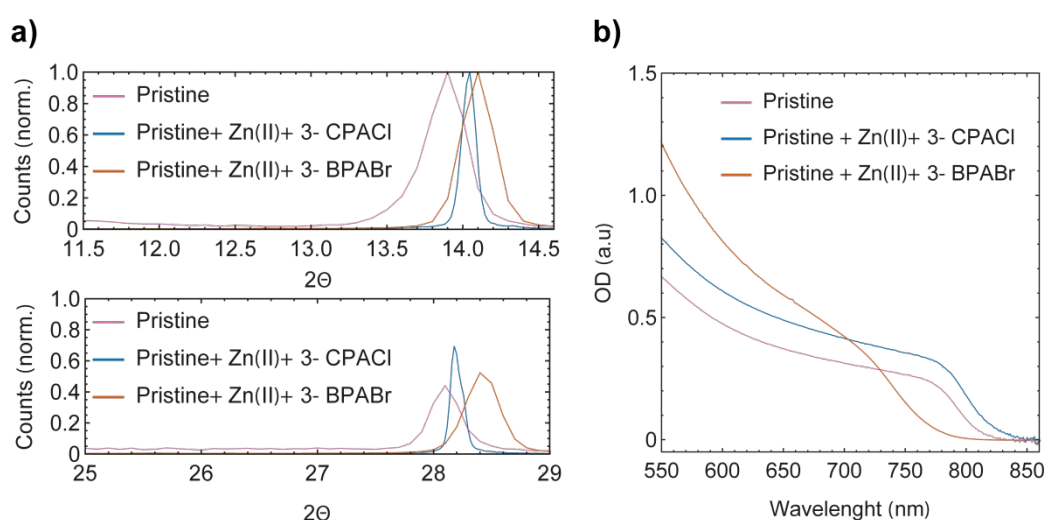


Figure 5. a) XRD patterns magnification for the (100) and (200) of the pristine material, pristine containing Zn(II) and 3-CPACl, and the one containing Zn(II) and

1
2
3 *3-BPABr. b) UV-Vis of the pristine material, the perovskite containing Zn(II) and*
4 *treated with 3-BPABr and 3-CPACl.*
5
6
7
8
9

10 For completeness, in **Figure S8** we report UV-Vis and XRD measurements of
11 freshly-made and aged pristine perovskite treated with only the film-forming agent 3-
12 CPACl. As shown, the resulting film is highly oriented along the (100) and (200) plane
13 and 6.3027Å as lattice parameter which implies a contraction of the unit cell. In terms
14 of stability, the material containing only 3-CPACl is stable after 60 days of exposure at
15 ambient conditions but it is only with a combination of the two additives that better
16 results are achieved.
17
18
19
20
21
22
23
24
25

26 The stable, doped perovskite containing Zn(II) and 3-CPACl can alternatively
27 be fabricated by a solid-solid reaction. The solid-solid reaction by grinding also works
28 for other perovskite materials³¹ (without additives or dopants) and pressing these
29 materials into pellets³² (or perovskite wafers)³³ has been applied before. Mixing the
30 precursor components (PbI₂, FAI, MABr, ZnI₂ and CPACl) in a vial by shaking induces
31 the reaction turning the material partly brown/black. The reaction can be completed by
32 grinding in a marble mortar under ambient conditions yielding a black material (**Figure**
33 **S9**). This indicates that the perovskite α -phase is thermodynamically favorable for this
34 composition, also in agreement with the phase-stability we observe for the final
35 perovskite. By using a simple KBr-press, the material can be turned into a perovskite
36 pellet that can undergo the same annealing procedure as the thin films.
37
38
39
40
41
42
43
44
45
46
47
48
49
50
51

52 We use the steady-state photoluminescence (PL) intensity to study the optical
53 quality of our films and correlate the introduction of Zn (II) and 3-CPACl with
54 photophysical properties of the film. PL data are normalized for the fraction of absorbed
55
56
57
58
59
60

1
2
3 photons at 485 nm (excitation wavelength) to account for any differences in the
4 absorption of the materials at that excitation wavelength. Relative to spin-coated layers
5 of pristine perovskite made and measured under the same conditions, the emission
6 intensity of the films containing Zn(II) incorporation is dramatically enhanced by an
7 order of magnitude and including 2% of 3-CPACl the intensity is even more boosted
8 (**Figure 6a** and **Table S2** for details). This implies that non-radiative recombination in
9 the perovskite layer has been significantly suppressed.

10
11
12 In addition, the PL peak position set at 1.55 eV does not show substantial shift for all
13 the compositions except for the one containing only the film-forming agent 3-CPACl
14 which shows a peak at 1.56 eV. Although it is not a significant shift, this might be due
15 to the presence of a small amount of chloride in the crystal lattice. The improved
16 stability, as result of noteworthy improvement of the quality of the films obtained, is
17 reflected in the photophysical properties as well.

18
19
20 Time Resolved Photoluminescence (TRPL) was carried out to elucidate how
21 the charge carrier dynamics of the pristine material changes with the introduction of
22 Zn(II) and 3-CPACl. The samples were excited with a 485 nm pulsed laser with
23 a repetition rate of 0.1 MHz. TRPL decay traces are fitted using a stretched
24 monoexponential function $f(t) = y_0 + \sum A_i e^{-\left(\frac{t}{\tau_1}\right)^\beta}$ where A_i is the amplitude, τ_1 is the
25 time constant and β is the stretch factor ranging between 0 and 1. Our motivation to
26 apply a stretched monoexponential function to these decays is that this model is
27 appropriate to describe the decay in heterogeneous materials showing monomolecular
28 recombination distributions which have already been observed in spatially-resolved PL
29 works for MAPbI₃ films^{34,35,36} but also for MAPbBr₃³⁷. Such effects can be induced
30 by differences in local material properties. Although the origin of these
31
32
33
34
35
36
37
38
39
40
41
42
43
44
45
46
47
48
49
50
51
52
53
54
55
56
57
58
59
60

heterogeneities and their effects on charge dynamics are still unknown, this is beyond the scope of our work.

The lifetime is found to be 588 ns for the pristine material, 634 ns when only Zn(II) is incorporated and 1547 ns when the film-forming 3-CPACl is applied in addition to Zn(II). This behavior is agreement with passivation mechanism of defects. Point defects such as vacancies ($V_{B^{2+}}$, V_{A^+} , V_{X^-}) and interstitials are dominant defects in ABX_3 perovskite.³⁸ Zinc (II) has a smaller ionic radius compared to Pb(II) and, as it is incorporated in the crystal lattice, fits in V_{pb} or interstitial sites to passivate defects. It might also be possible that the decreases in the bulk defect density is a consequence of the increase of the formation energy of defects. Furthermore, the reduction of grain boundaries due to grains enlargement induced by the 3-CPACl reduce the amount of dangling bonds, which are usually present in those regions, improving the overall quality of the film.

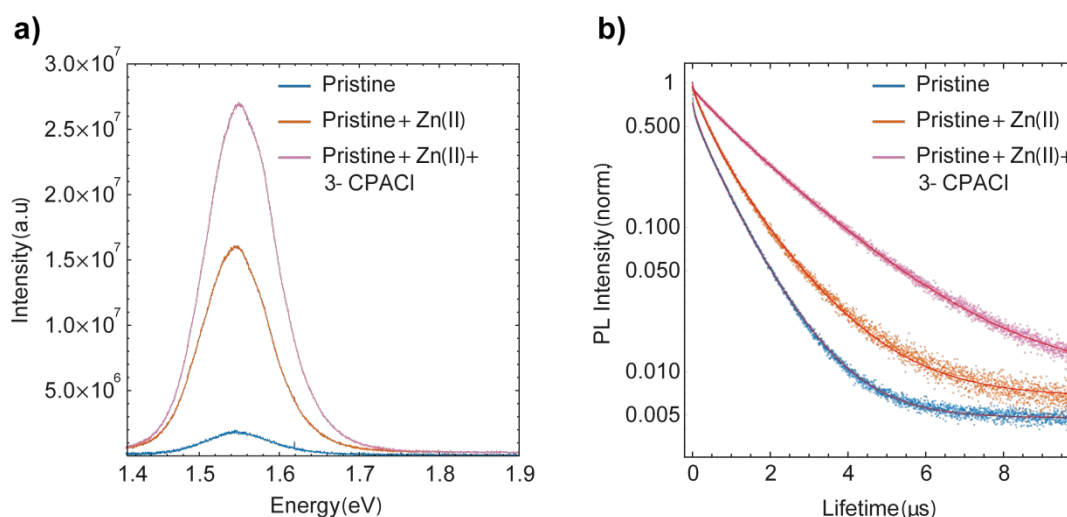


Figure 6. a) Steady-state PL of the three compositions explored. The excitation wavelength used is 485 nm. **b).** Time-resolved PL decay of after the three compositions used with excitation wavelength at 485 nm and 0.1 MHz excitation frequency.

Summary

We have shown that mixed FA/MA cations and mixed halides (Br/I) lead perovskite for solar cells, fabricated under ambient conditions, can be stabilized by the introduction of 2.5% of ZnI₂. By XRD, Zn(II) is proven to be incorporated in the perovskite structure despite its smaller ionic radius compared to Pb(II). UV-Vis and XRD comparison of freshly-made and aged samples containing Zn(II) show the same behaviour after 14 days of storage under ambient conditions. The incorporation of Zn(II) affects also photophysical properties of the perovskite as the PL emission is enhanced of one order of magnitude in agreement with passivation mechanism of defects and the lifetime is prolonged from 588 ns (for the pristine material) to 634 ns. In addition, to obtain dense, pinhole-free layers we applied a chloroamine hydrochloride additive, 3-CPACl. The introduction of this additive in the precursor solution results in a straightforward method to obtain reproducible and highly crystalline oriented layers along the (100) and (200) crystallographic direction. Larger grains, homogeneous and more compact layers are also observed in SEM images. Using Zn(II) and 3-CPACl in combination, the photoluminescence is enhanced with respect to the composition containing only Zn(II) and the lifetime extended to 1547 ns. We want to highlight the intriguing effect of including a transition metal as Zn(II) in the perovskite lattice also for perovskite fabricated under ambient conditions. Further work is needed to optimize the device interfaces and architecture to obtain more efficient solar cells under ambient conditions. We are optimistic that the one-step fabrication in air, together with the excellent stability enhanced by incorporation of Zn(II) and 3-CPACl, will spark these optimization efforts.

Supporting Information

Images of the sample containing Zn(II) and 3-CPACl during spin-coating deposition; Uv-Vis and XRD measurements of the pure $(\text{FA}_{0.85}\text{MA}_{0.15})\text{Pb}(\text{I}_{0.85}\text{Br}_{0.15})_3$ and the same material containing only the hydrochloride additive ; XRD of the film containing 5 wt% of Zn(II); Solid-solid reaction completed by ambient grinding; EDX spectrum of the film containing Zn(II) and 3-CPACl; XRD of the film containing Zn(II) and 3-CPACl on PEDOT:PSS; SEM image for the pristine material and the one containing only $\text{Zn}(\text{II})_3$; Table with crystallite sizes for each composition; Table with photoluminescence data for each composition.

Acknowledgements

We thank the Erasmus+ exchange program for supporting LAM, RJC, OL and CM. We thank Prof. Dr. Ir. R. A. J. Janssen for solar cell research facilities, Universiteit van Amsterdam for structural support and Hysen Drogu for graphical design in Figure 3. This work is part of the research program of the Netherlands Organisation for Scientific Research (NWO) and was partly performed at the research institute AMOLF.

References

- (1) Kojima, A.; Teshima, K.; Shirai, Y.; Miyasaka, T. Organometal Halide Perovskites as Visible-Light Sensitizers for Photovoltaic Cells. *J. Am. Chem. Soc.* **2009**, *131* (17), 6050–6051.
- (2) Polman, A.; Knight, M.; Garnett, E. C.; Ehrler, B.; Sinke, W. C. Photovoltaic Materials: Present Efficiencies and Future Challenges. *Science*. **2016**, *352* (6283).

- 1
2
3 (3) Stoumpos, C. C.; Malliakas, C. D.; Kanatzidis, M. G. Semiconducting Tin and
4 Lead Iodide Perovskites with Organic Cations: Phase Transitions, High
5 Mobilities, and Near-Infrared Photoluminescent Properties. *Inorg. Chem.* **2013**,
6 52 (15), 9019–9038.
7
8
9
10
11
12 (4) Baikie, T.; Fang, Y.; Kadro, J. M.; Schreyer, M.; Wei, F.; Mhaisalkar, S. G.;
13 Graetzel, M.; White, T. J. Synthesis and Crystal Chemistry of the Hybrid
14 Perovskite (CH₃NH₃)PbI₃ for Solid-State Sensitised Solar Cell Applications.
15 *J. Mater. Chem. A* **2013**, 1 (18), 5628–5641.
16
17
18
19
20
21 (5) Gélvez-Rueda, M. C.; Renaud, N.; Grozema, F. C. Temperature Dependent
22 Charge Carrier Dynamics in Formamidinium Lead Iodide Perovskite. *J. Phys.*
23 *Chem. C* **2017**, 121 (42), 23392–23397.
24
25
26
27
28 (6) Weber, D. CH₃NH₃PbX₃, Ein Pb(II)-System Mit Kubischer
29 Perowskitstruktur. **2015**, 1445 (August 1978), 1443–1445.
30
31
32
33 (7) Hui, Y.; Feng, W.; Fangyan, X.; Wenwu, L.; Jian, C.; Ni, Z. The Role of
34 Chlorine in the Formation Process of “CH₃NH₃PbI₃-xCl_x” Perovskite. *Adv.*
35 *Funct. Mater.* **2014**, 24 (45), 7102–7108.
36
37
38
39
40 (8) Yang, W. S.; Noh, J. H.; Jeon, N. J.; Kim, Y. C.; Ryu, S.; Seo, J.; Seok, S. Il.
41 High-Performance Photovoltaic Perovskite Layers Fabricated through
42 Intramolecular Exchange. *Science* **2015**, 348 (6240), 1234-1237.
43
44
45
46 (9) Saliba, M.; Matsui, T.; Seo, J.-Y.; Domanski, K.; Correa-Baena, J.-P.;
47 Nazeeruddin, M. K.; Zakeeruddin, S. M.; Tress, W.; Abate, A.; Hagfeldt, A.;
48 Grätzel, M. Cesium-Containing Triple Cation Perovskite Solar Cells: Improved
49 Stability, Reproducibility and High Efficiency. *Energy Environ. Sci.* **2016**, 9
50 (6), 1989–1997.
51
52
53
54
55
56
57
58 (10) Saliba, M.; Matsui, T.; Domanski, K.; Seo, J.-Y.; Ummadisingu, A.;
59
60

- 1
2
3 Zakeeruddin, S. M.; Correa-Baena, J.-P.; Tress, W. R.; Abate, A.; Hagfeldt, A.;
4
5 Grätzel, M. Incorporation of Rubidium Cations into Perovskite Solar Cells
6
7 Improves Photovoltaic Performance. *Science* **2016**, 354 (6309), 206-209.
8
9
- (11) Abdi-Jalebi, M.; Dar, M. I.; Sadhanala, A.; Senanayak, S. P.; Franckevičius,
10
11 M.; Arora, N.; Hu, Y.; Nazeeruddin, M. K.; Zakeeruddin, S. M.; Grätzel, M.;
12
13 Friend, R. H. Impact of Monovalent Cation Halide Additives on the Structural
14
15 and Optoelectronic Properties of CH₃NH₃PbI₃ Perovskite, *Adv. Energy Mater.*
16
17 **2016**, 61502472.
18
19
- (12) Wang, J. T. W.; Wang, Z. P.; Pathak, S.; Zhang, W.; deQuilettes, D. W.;
20
21
22 Wisnivesky-Rocca-Rivarola, F.; Huang, J.; Nayak, P. K.; Patel, J. B.; Yusof, H.
23
24 A. M.; Vaynzof, Y.; Zhu, R.; Ramirez, I.; Zhang, J.; Ducati, C.; Grovenor, C.;
25
26 Johnston, M. B.; Ginger, D. S.; Nicholas, R. J.; Snaith, H. Efficient Perovskite
27
28 Solar Cells by Metal Ion Doping. *Energy Environ. Sci.* **2016**, 9 (9), 2892–2901.
29
30
- (13) Pérez-del-Rey, D.; Forgács, D.; Hutter, E. M.; Savenije, T. J.; Nordlund, D.;
31
32
33 Schulz, P.; Berry, J. J.; Sessolo, M.; Bolink, H. J. Strontium Insertion in
34
35 Methylammonium Lead Iodide: Long Charge Carrier Lifetime and High Fill-
36
37 Factor Solar Cells *Adv. Mater.* **2016**, 28 (44), 9839–9845.
38
39
- (14) Klug, M. T.; Osherov, A.; Haghighirad, A. A.; Stranks, S. D.; Brown, P. R.;
40
41
42 Bai, S.; Wang, J. T. W.; Dang, X. N.; Bulovic, V.; Snaith, H. J.; Belcher, A. M.
43
44 Tailoring Metal Halide Perovskites through Metal Substitution: Influence on
45
46 Photovoltaic and Material Properties. *Energy Environ. Sci.* **2017**, 10 (1), 236–
47
48 246.
49
50
- (15) van der Stam, W.; Geuchies, J. J.; Altantzis, T.; van den Bos, K. H. W.;
51
52
53 Meeldijk, J. D.; Van Aert, S.; Bals, S.; Vanmaekelbergh, D.; de Mello Donega,
54
55
56 C. Highly Emissive Divalent-Ion-Doped Colloidal CsPb_{1-x}MxBr₃ Perovskite
57
58
59
60

- 1
2
3 Nanocrystals through Cation Exchange. *J. Am. Chem. Soc.* **2017**, *139* (11),
4 4087–4097.
5
6
7
8 (16) Jin, J.; Li, H.; Chen, C.; Zhang, B.; Xu, L.; Dong, B.; Song, H.; Dai, Q.
9
10 Enhanced Performance of Perovskite Solar Cells with Zinc Chloride Additives.
11
12 *ACS Appl. Mater. Interfaces* **2017**, *9* (49), 42875–42882.
13
14 (17) Wang, Y.; Song, N.; Feng, L.; Deng, X. Effects of Organic Cation Additives on
15
16 the Fast Growth of Perovskite Thin Films for Efficient Planar Heterojunction
17
18 Solar Cells. *ACS Appl. Mater. Interfaces* **2016**, *8* (37), 24703–24711.
19
20
21 (18) Wang, F.; Geng, W.; Zhou, Y.; Fang, H.-H.; Tong, C.-J.; Loi, M. A.; Liu, L.-
22
23 M.; Zhao, N. Phenylalkylamine Passivation of Organolead Halide Perovskites
24
25 Enabling High-Efficiency and Air-Stable Photovoltaic Cells *Adv. Mater.* **2016**,
26
27 *28* (45), 9986–9992.
28
29
30 (19) Jeon, N. J.; Noh, J. H.; Yang, W. S.; Kim, Y. C.; Ryu, S.; Seo, J.; Seok, S. Il.
31
32 Compositional Engineering of Perovskite Materials for High-Performance
33
34 Solar Cells. *Nature* **2015**, *517* (7535), 476–480.
35
36
37 (20) Li, C.; Lu, X.; Ding, W.; Feng, L.; Gao, Y.; Guo, Z. Formability of ABX₃ (X =
38
39 F, Cl, Br, I) halide perovskites *Acta Crystallogr. Sect. B* **2008**, *64* (6), 702–707.
40
41
42 (21) Wang, S.; Jiang, Y.; Juarez-Perez, E. J.; Ono, L. K.; Qi, Y. Accelerated
43
44 Degradation of Methylammonium Lead Iodide Perovskites Induced by
45
46 Exposure to Iodine Vapour. *Nat. Energy* **2016**, *2*, 16195.
47
48
49 (22) Niu, G.; Li, W.; Meng, F.; Wang, L.; Dong, H.; Qiu, Y. Study on the Stability
50
51 of CH₃NH₃PbI₃ Films and the Effect of Post-Modification by Aluminum
52
53 Oxide in All-Solid-State Hybrid Solar Cells. *J. Mater. Chem. A* **2014**, *2* (3),
54
55 705–710.
56
57
58 (23) Zhang, W.; Pathak, S.; Sakai, N.; Stergiopoulos, T.; Nayak, P. K.; Noel, N. K.;
59
60

- Haghighirad, A. A.; Burlakov, V. M.; deQuilettes, D. W.; Sadhanala, A.; Li, W.; Wang, L.; Ginger, D. S.; Friend, R. H.; Snaith, H. J. Enhanced Optoelectronic Quality of Perovskite Thin Films with Hypophosphorous Acid for Planar Heterojunction Solar Cells. *Nat. Commun.* **2015**, *6* (May), 1–9.
- (24) Williams, S. T.; Zuo, F.; Chueh, C.-C.; Liao, C.-Y.; Liang, P.-W.; Jen, A. K.-Y. Role of Chloride in the Morphological Evolution of Organo-Lead Halide Perovskite Thin Films. *ACS Nano* **2014**, *8* (10), 10640–10654.
- (25) Chueh, C.-C.; Liao, C.-Y.; Zuo, F.; Williams, S. T.; Liang, P.-W.; Jen, A. K.-Y. The Roles of Alkyl Halide Additives in Enhancing Perovskite Solar Cell Performance. *J. Mater. Chem. A* **2015**, *3* (17), 9058–9062.
- (26) Chen, Y.; Zhao, Y.; Liang, Z. Non-Thermal Annealing Fabrication of Efficient Planar Perovskite Solar Cells with Inclusion of NH₄Cl. *Chem. Mater.* **2015**, *27* (5), 1448–1451.
- (27) Wang, F.; Yu, H.; Xu, H.; Zhao, N. HPbI₃: A New Precursor Compound for Highly Efficient Solution-Processed Perovskite Solar Cells. *Adv. Funct. Mater.* **2015**, *25* (7), 1120–1126.
- (28) Noel, N. K.; Congiu, M.; Ramadan, A. J.; Fearn, S.; McMeekin, D. P.; Patel, J. B.; Johnston, M. B.; Wenger, B.; Snaith, H. J. Unveiling the Influence of PH on the Crystallization of Hybrid Perovskites, Delivering Low Voltage Loss Photovoltaics. *Joule* **2017**, *1* (2), 328–343.
- (29) Mitzi, D. B.; Feild, C. A.; Harrison, W. T. A.; Guloy, A. M. Conducting Tin Halides with a Layered Organic-Based Perovskite Structure. *Nature* **1994**, *369*, 467.
- (30) Chen, Q.; Zhou, H.; Fang, Y.; Stieg, A. Z.; Song, T.-B.; Wang, H.-H.; Xu, X.; Liu, Y.; Lu, S.; You, J.; Sun, P.; McKay, J.; Goorsky, M. S.; Yang, Y. The

- 1
2
3 Optoelectronic Role of Chlorine in CH₃NH₃PbI₃(Cl)-Based Perovskite Solar
4 Cells. *Nat. Commun.* **2015**, *6*, 7269.
- 5
6
7
8 (31) Zhu, Z.-Y.; Yang, Q.-Q.; Gao, L.-F.; Zhang, L.; Shi, A.-Y.; Sun, C.-L.; Wang,
9 Q.; Zhang, H.-L. Solvent-Free Mechanochemistry of Composition-Tunable
10 Cesium Lead Halide Perovskite Quantum Dots. *J. Phys. Chem. Lett.* **2017**, *8*
11 (7), 1610–1614.
- 12
13
14
15
16
17 (32) Guerrero, A.; Garcia-Belmonte, G.; Mora-Sero, I.; Bisquert, J.; Kang, Y. S.;
18 Jacobsson, T. J.; Correa-Baena, J.-P.; Hagfeldt, A. Properties of Contact and
19 Bulk Impedances in Hybrid Lead Halide Perovskite Solar Cells Including
20 Inductive Loop Elements. *J. Phys. Chem. C* **2016**, *120* (15), 8023–8032.
- 21
22
23
24
25
26 (33) Shrestha, S.; Fischer, R.; Matt, G. J.; Feldner, P.; Michel, T.; Osvet, A.;
27 Levchuk, I.; Merle, B.; Golkar, S.; Chen, H.; Tedde, S. F. High-Performance
28 Direct Conversion X-Ray Detectors Based on Sintered Hybrid Lead Triiodide
29 Perovskite Wafers. *Nat. Photonics* **2017**, *11*, 436.
- 30
31
32
33
34
35 (34) Nie, W.; Tsai, H.; Asadpour, R.; Blancon, J.-C.; Neukirch, A. J.; Gupta, G.;
36 Crochet, J. J.; Chhowalla, M.; Tretiak, S.; Alam, M. A.; Wang, H.-L.; Mohite,
37 A. D. High-Efficiency Solution-Processed Perovskite Solar Cells with
38 Millimeter-Scale Grains. *Science* **2015**, *347* (6221), 522–525.
- 39
40
41
42
43
44 (35) Vinet, L.; Zhedanov, A. Impact of Micro Structure on Local Carrier Lifetime in
45 Perovskite Solar Cells. *J. Phys. A Math. Theor.* **2011**, *44* (8), 085201.
- 46
47
48
49 (36) Draguta, S.; Thakur, S.; Morozov, Y. V.; Wang, Y.; Manser, J. S.; Kamat, P.
50 V.; Kuno, M. Spatially Non-Uniform Trap State Densities in Solution-
51 Processed Hybrid Perovskite Thin Films. *J. Phys. Chem. Lett.* **2016**, *7* (4), 715–
52 721.
- 53
54
55
56
57
58 (37) Vrućinić, M.; Matthiesen, C.; Sadhanala, A.; Divitini, G.; Cacovich, S.; Dutton,
59
60

- 1
2
3 S. E.; Ducati, C.; Atatüre, M.; Snaith, H.; Friend, R. H.; Sirringhaus, H.;
4
5 Deschler, F. Local Versus Long-Range Diffusion Effects of Photoexcited
6
7 States on Radiative Recombination in Organic-Inorganic Lead Halide
8
9 Perovskites. *Adv. Sci.* **2015**, *2*, 1500136.
10
11
12 (38) Buin, A.; Pietsch, P.; Xu, J.; Voznyy, O.; Ip, A. H.; Comin, R.; Sargent, E. H.
13
14 Materials Processing Routes to Trap-Free Halide Perovskites. *Nano Lett.* **2014**,
15
16 *14* (11), 6281–6286.
17
18
19
20
21
22
23
24
25
26
27
28
29
30
31
32
33
34
35
36
37
38
39
40
41
42
43
44
45
46
47
48
49
50
51
52
53
54
55
56
57
58
59
60

1
2
3
4
5
6
7
8 **Table of Contents graphic**
9

